GaAs manufacturing processes conditions for micro- and nanoscale devices

F. Joint, C. Abadie, P.B. Vigneron, L. Boulley, F. Bayle, N. Isac, A. Cavanna, E. Cambril, E. Herth

Version of Record: https://www.sciencedirect.com/science/article/pii/S1526612520307805
Manuscript_c90bc0c020c0614884c0ea8a09a32c70

ELSEVIER

Available online at www.sciencedirect.com

ScienceDirect

Journal of Manufacturing Processes 00 (2020) 1–10

Manufacturing Processes

GaAs manufacturing processes conditions for micro- and nanoscale devices

F. Joint[a,b], C. Abadie[a], PB. Vigneron[a,c], L. Boulley[a], F. Bayle[a], N. Isac[a], A. Cavanna[a], E. Cambril[a], E. Herth[a]

etienne.herth@c2n.upsaclay.fr

[a]*Centre de Nanosciences et de Nanotechnologies, CNRS UMR 9001, Univ. Paris-Sud, Université Paris-Saclay, Palaiseau, France.*
[b]*Center for Nanophysics and Advanced Materials, Department of Physics, University of Maryland, College Park, Maryland 20742, USA.*
[c]*Edward L. Ginzton Laboratory, Stanford University, Stanford, California 94305, USA.*

Abstract

High aspect-ratio etchings are a key aspect of the fabrication of III-V semiconductor devices. The increasing demand for diverse geometries with various characteristic lengths (from the micro- to the nano-meter scale) requires the constant development of new etching recipes. In this article, we demonstrate a versatile mask-plasma combination for micro- and nanofabrication of GaAs substrate using an Inductive Coupled Plasma-Reactive Ion Etching (ICP-RIE) system. We identify five recipes at 25 °C, with high selectivity, and apply them on one photoresist (AZ4562) and two hard (Chromium and Nickel) masks. The optimized etching plasma chemistry ($BCl_3/Cl_2/Ar/N_2$) shows a pattern transfer on GaAs with a high rate (≥5.5 μm/min), a high anisotropy, a high selectivity (>4:1 with photoresist mask, and >50:1 with hard masks), a good etch surface morphology, and smooth sidewalls profile (>88°). Herein, we detail the requirements definition, the engineering processes with detailed recipes, the verification, and validation of three device geometries (ridges, cylinders, and nanopillars). The presented results can be valuable for a wide range of applications from the microscale to the nanoscale, and are compatible with a manufacturing process using only a single commercial ICP-RIE tool with two chambers dedicated, respectively, for metallic masks and photoresist mask.

Keywords: Microfabrication, Nanofabrication, Dry etching, Chlorine plasma

1. Introduction

Micro- and nanotechnologies using ICP-RIE technology are widely used in both manufacturing and research laboratories [1, 2, 3, 4]. III-V semiconductors suit high performance applications beyond optoelectronics due to the higher electron mobilities and peak velocities compared to silicon based devices [5, 6, 7]. However, the different processing techniques on III-V materials are still challenging and needs further developments. For instance, there is a growing interest for the advancement of reliable plasma etching technics on III-V materials for electronic and photonic applications. ICP-RIE etching technology enables plasma etching to operate at lower pressures (1-30 mTorr) with anistropic features and etch rates comparable to or higher than conventional reactive-ion etching (RIE) [8, 9, 10, 11, 12]. There have been numerous reports on the etching of silicon [12, 13, 14] and semiconductor devices based on GaAs/AlGaAs, which are widely used for the fabrication of microsystems [15, 16], electronic and photonic devices [17, 18, 19]. These various applications require high etching rates, anisotropic etching profiles, smooth sidewalls and good surface morphology in the microscale as well as in the nanoscale. However, the critical manufacturing step to obtain nearly perfect anisotropic profiles, with respect to the various devices, is sensitive to the choice of both plasma etching chemistry and masking material. Therefore, the latter needs to be finely selected and tuned.

Conventional III-V compounds etch masks consist of hard masks based on metals [20], dielectric layers (silicon oxide or silicon nitride) [21] and thick photoresists [22, 23]. Some mask materials adapted to chlorine chemistry processes already exist but little is known about the reliability of these materials used for pattern transfer on III-V compounds, particularly concerning the defects encountered during the micro- and nanofabrication. Since the mask interacts with the plasma, it is crucial to understand each mask behavior to obtain a high fidelity pattern textcolorredtransfer on the III-V compounds over the entire etching period. Moreover, information on the etching rate and selectivity for each mask enables a better and reliable manufacturing process. Several investigations on etchants targeting specific materials have been made but would only report on the etching rates on III-V compounds, and would rarely

discuss the selectivity of the mask transfer from microscale towards nanoscale (viz. GaAs vs mask transfer layer). At the micrometer scale, the degree of anisotropy can be improved by adding inert gases such as argon (Ar) with a mixture of Cl_2, BCl_3 gases on GaAs/AlGaAs substrate [24, 25]. In contrast, at the nanometer scale, the choice of an ideally balanced BCl_3/Cl_2/Ar chemistry is difficult to obtain due to under etching [26]. To protect the sidewalls, N_2 gas is added into BCl_3/Cl_2/Ar plasma. The presence of N_2 also improves the selectivy, cleans the surfaces, and maintains a high anisotropy for different scale ranges [27, 28, 29, 30, 31].We have previously demonstrated the feasibility of the chlorine-based GaAs/AlGaAs etch plasma chemistries at the microscale [32] and we have improved the etch rate, the selectivity, the quality of sidewall surfaces and the verticality of the ridge structure commonly used for quantum cascade lasers [18]. Nevertheless, the lack of knowledge in how to apply and integrate engineering processes from microscale towards nanoscale technologies is an obstacle to the selection of specific plasmas in dry etching systems. Hence, we develop in this article manufacturing engineering methodologies that integrate the chlorinated plasma chemistry to obtain with high reliable microdevices and nanodevices of predetermined shapes.

We demonstrate that the desired etching characteristics on GaAs, meaning vertical sidewalls, very low or insignificant roughness on the surface sidewalls, can be obtained in ICP-RIE with a $BCl_3/Cl_2/Ar/N_2$ plasma chemistry and using a photoresist mask or a selected hard mask. We present here the different mask transfer methods and etching recipes which allow to obtain straight and smooth sidewalls at the nanoscale supported by GaAs etching profiles analysis.

2. Experimental section

The experiments were performed in a Surface Technology Systems (STS) reactor, equipped with a maximum available power of 900 W, 13.56 MHz RF coil generator. The gases employed in this study were BCl_3, Cl_2, Ar, N_2 and O_2. During all the experiments, the temperature of the electrode was fixed at 25 °C. To avoid contamination of the ICP reactor using exclusively chlorine chemistries, two chambers are dedicated separately for metallic masks and photoresist mask. A 5-min-long oxygen cleaning procedure was performed between each run to remove any polymer from the reactor sidewalls, minimizing contaminations, and preserving process repeatability. The samples were loaded into the reactor by mounting them on an 8" (200 mm) alumina (Al_2O_3) carrier wafer with "glue" (vacuum grease) to enhance good thermal contact. As part of the optimization of the etching parameters, a mask designed with different kinds of test structures (trenches and cavities) to help characterizing the process outcome was employed. In this investigation, an inspection of the resulting dry etching parameters (etching rates, profiles, surface qualities and selectivities) was the best way to check the quality of our etching process. All test samples were 1 cm x 1 cm pieces of bulk (100) GaAs oriented. In this study, the ratio of the coil power /platen power (P_{ICP} / P_{Bias}) was fixed to 8:1, for 800 W P_{ICP}, and 80 W P_{Bias}. Selected typical parameters from those of the optimized processes presented in our previous work [32] are summarized in Table I, with the recipes (T) abbreviated names.

The samples were characterized using an optical microscope and a Scanning Electron Microscope (SEM). The mask selectivity was estimated by calculating the ratio of the semiconductor etching rate to the photoresist or hard masks etching rates.

Table 1. Typical parameters from the different etching processes used in this study with coil power: platen power fixed to 8:1. [32]

		Gas Flow rate (sccm)				
Recipe	P (mTorr)	BCl_3/Cl_2	BCl_3	Cl_2	Ar	N_2
T1	10	6	15	2.5	5	3
T2	10	20	50	2.5	5	3
T3	20	20	50	2.5	5	5
T4	30	20	50	2.5	5	3
T5	30	20	50	2.5	5	5

3. Results

3.1. Microscale

There are numerous important parameters which affect the etching process such as etching rate, masking materials, selectivity and surface roughness. Kovacs *et. al* [33] provide with a general comparison between different etchants properties regarding the aforementioned important etching characteristics required. They also discussed about the suitable masking materials for such etching processes. In our work, micro- and nanometer-sized patterns were fabricated using a top-down approach with an organic or inorganic mask, combining lithographic methods (viz. lift-off), metal deposition and dry etching. This allowed us to obtain well-controlled densities, diameters, spacing and spatial positions. Fig.1a-d presents the flow chart of the process using the 6 μm-thick photoresist AZ4562, as the organic mask material to pattern and transfer test geometries on GaAs wafers at the microscale. The wafer was then cleaved in different samples and further set into little batches (1 cm^2) for the different investigated recipes. After the etching process, each samples were cleaved perpendicular to the trenches axis to observe their profiles.

In contrast to pure Cl_2 plasma etching on GaAs, where undercut etching occurs, Franz *et al.* [34] reported that the addition of BCl_3 to Cl_2 enables to easily obtain vertical sidewalls due to the phenomenon of sidewall passivation by formation of the polymer B_2Cl_4. The addition of BCl_3 increases the etching rate significantly because it facilitates chlorine ions generation according to the following equation :

$$BCl_3^* + Cl_2 \longrightarrow BCl_4^- + Cl^+ \quad (1)$$

Pearton *et al.* extensively investigated the effect of a small addition of the inert gas N_2 to BCl_3/Cl_2 chemistries to induce sidewall protection when using a UV photoresist mask [27]. Other studies confirm that with these adjusted chemistries,

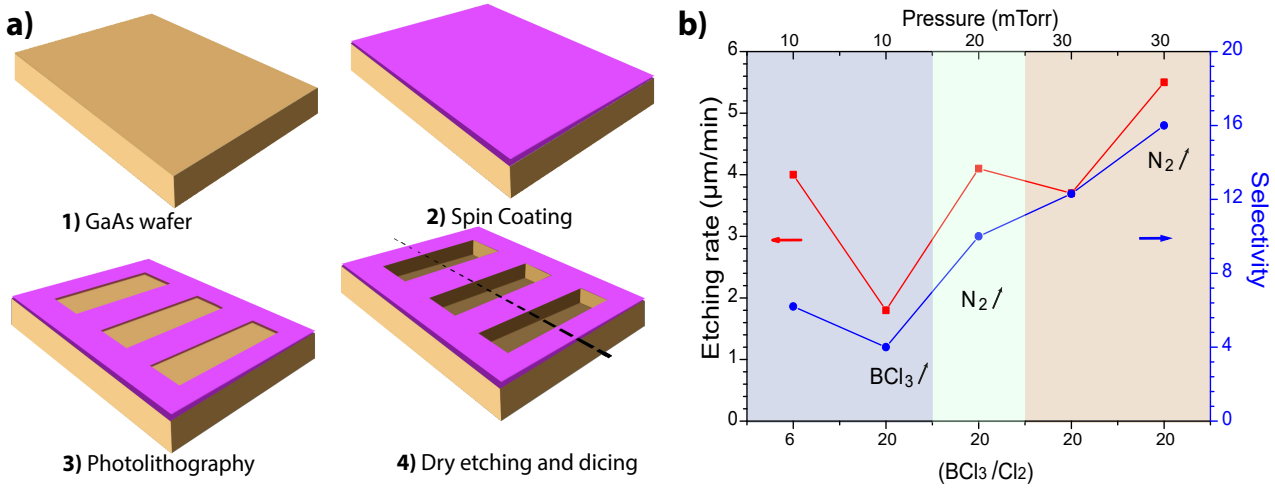

Figure 1. a) Flowchart of the GaAs trenches manufacturing process, and (b) etching rate of GaAs and the resist selectivity as function of the BCl_3/Cl_2 gas ratio from Table 1.

straight and smooth sidewalls can be obtained on other substrates such as InP and GaN [35, 36, 21]. Furthermore, previous works on GaAs/AlGaAs heterostructure have shown that the addition of Ar to the $BCl_3/Cl_2/N_2$ mix can improve the degree of control of the anisotropy [27, 21, 32]. As presented in Fig.1b, we observed that the etch rate (red curve) increases gradually from 1.8 μm/min to 5.5 μm/min, when the pressure is raised from 10 mTorr (recipe T2) to 30 mTorr (recipe T5). The increase in the etch rate for higher pressure is attributed to an increase in the concentration of reactive chlorine species which enhances the etching capacity of the chemical components. , Increasing the pressure can improve the selectivity (blue curve) on the photoresist mask than lower pressure. Photoresist masks offer the simplicity of a single processing step with a good selectivity, approximately 4:1 at 10 mTorr and 16:1 at 30 mTorr. Therefore, it is possible to use a thinner layer of photoresist on GaAs substrates in higher pressure conditions. The latter eases the photolithographic patterning of the transfer mask with small dimensions.

For microsystem applications, several additional etching profile defects must be avoided, among them bowing, notching, micro-trenching and non flat bottom surfaces. Fig.2 shows the cross section of the trenches obtained for different process recipes (see Table I). We observe that the bowing effect is sensitive to the mask opening size as seen in Fig.2a, and it improves for the largest mask openings provided that the ratio of gas mixture BCl_3/Cl_2 is around 20. When the pressure increases up to 30 mTorr (T4), sidewall passivation deteriorates and bowing effects appear. This problem can be limited by increasing the N_2 flow rate (T5), as observed in Fig.2b. The process T5, at 30 mTorr, with BCl_3/Cl_2 ratio of 20:1 and adjunction of 5 sccm of N_2 gas is adapted for microfabrication devices that require high aspect ratio and good profile control as this recipe presents low bowing effects on the side walls. This recipe also has the advantage of providing high etching speed and a good selectivity on resist masks. In general, the resist-mask obtained with photo-

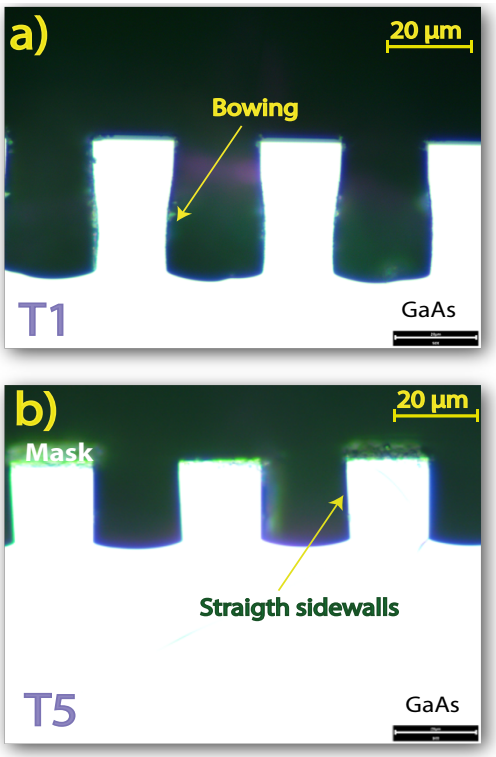

Figure 2. Cross-section of the trenches obtained for two process recipes :(a) T1, and (b) T5. The profiles were etched at different pressures 10 mTorr and 30 mTorr, see the corresponding recipe in Table I, and presented in Fig.1(e).

lithography must be transferred vertically. However, the sidewall angle formed between the top of the substrate and the resist is never perfectly 90°, the resist could recess with the directive etching plasma and expose the top of the substrate ridges, leading to deterioration (ie roughness). To avoid the roughness sidewalls, the resist thickness is chosen so that only half of the resist is consumed during the etching process. The minimum

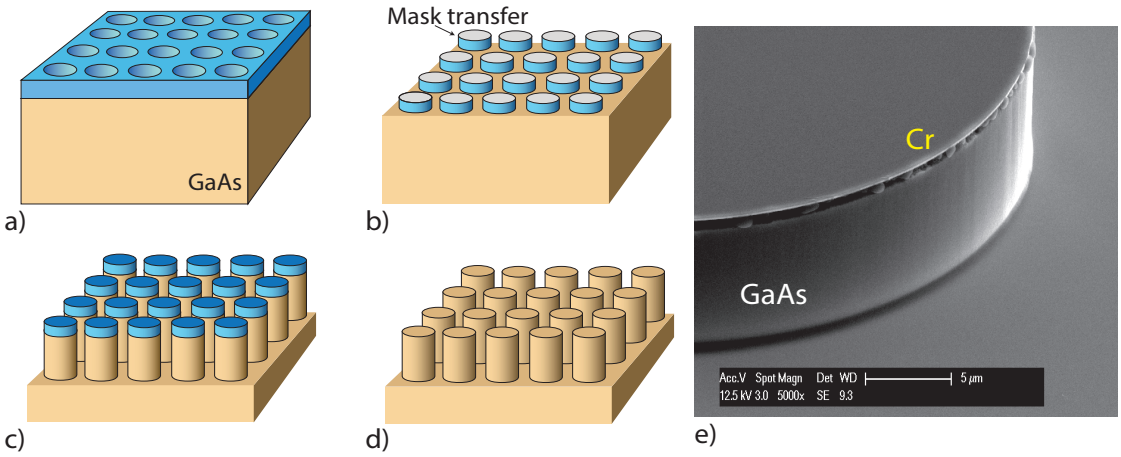

Figure 3. Flowchart of the microdevices manufacturing process: (a)-(b) Metal Lift-off; (c) plasma etching surface, (d) mask removal, and e) SEM micrographs of the microdisk transferred from a Cr-mask to the GaAs substrate using T2 recipe. The spacing between each disk grouping was 100 μm with diameter of 30, 50 and 80 μm.

resist-thickness is governed by the equation:

$$T_{min} > 2 \times [\frac{H}{S_{mask}}] \quad (2)$$

where T_{min} is the required minimum thickness of the mask transfer in order to avoid faceting as well as rough sidewalls, H is the desired etching depth, and S_{mask} is the selectivity of the mask tranfer to that of the etching substrate.

Therefore, deeper etching requires thicker photoresist masks during prolonged process but the resolution of the photolithography pattern transfer is then limited. Although thick photoresist-protected microstructures using chlorine-based chemistries (BCl_3 and/or Cl_2) with N_2 are attractive, they cannot be adapted to the fabrication of submicron devices. The challenges in the nanotechnology scale are very different and need to be adjusted in consideration. In the next section, we investigate the effect of hard mask for the manufacturing of microdevices as well as nanodevices to improve the selectivity.

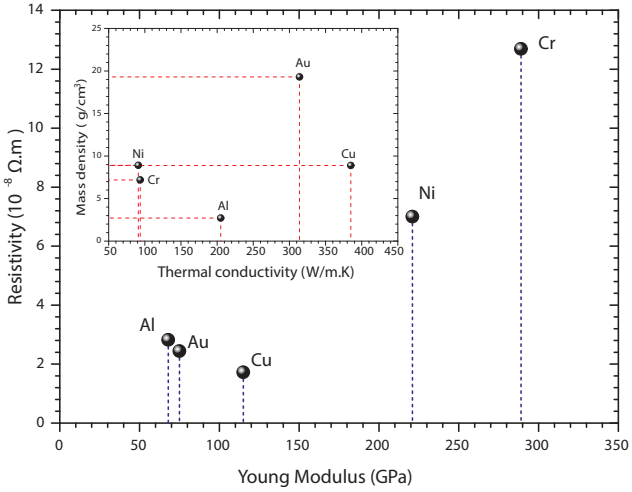

Figure 4. Physical properties of the common mask materials used in dry etching chemistry, where ρ, E, and D are respectively the resistivity, the Young modulus and the mass density [40].

3.2. Nanoscale

The increasing interest for the nanoscale has been focused on GaAs nanopillars for various applications including solar cells [29], nano-lasers [5], light emitting diodes [37] and others [38, 39]. However, the main difficulty in nanodevices manufacturing lies in their dimensions: obtaining nanodevices with vertical sidewalls of several μm of depth, high aspect ratio and smooth surfaces remains a technological challenge. It is well known that deeper etching is not easy with thinner tone-resist masks due to low selectivity and mask profile degradation during a prolonged process. We have opted for the use of metal masks for the nano-device fabrication process.

In this section, we manufactured micro-disks in order to validate (Fig.3) the quality of the sidewall's quality at the microscale and to pre-select recipes that might be used at the nanoscale. In Nanoscale, we have used a process combining electronic beam lithography (EBL) and a lift-off processes to create metal pattern on GaAs substrate [41, 42, 43, 44]. Fig.3a-d presents the process steps for the inorganic masks obtained with the deposition of a thin metal layer and a lift-off in acetone at the microscale and nanoscale. Due to the brittle nature of the material (thin layer and mechanical properties), the metal cleanly fractures and easily lifts off. Based on the flow chart presented in Fig.3, the starting mask was composed of 30 μm to 80 μm diameter disks obtained by optical lithography and nano-disks with diameters ranging from 450 nm to 550 nm processed with EBL. The pitch between the nanodisks was 10 μm x 20 μm. All the samples at the microscale were etched five minutes whereas at the nanoscale, the etching time was reduced to the range from 60 to 100 seconds due to a thinner mask layer and a high aspect ratio.

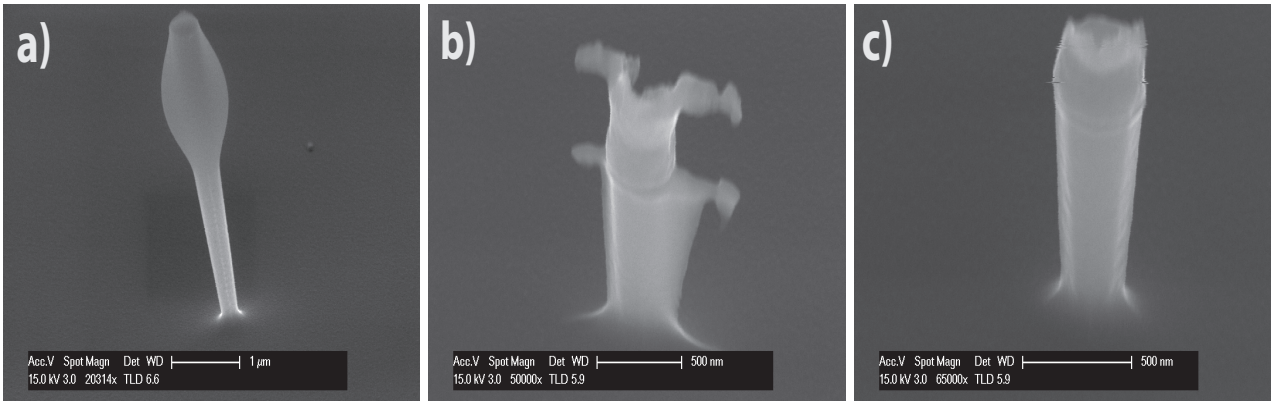

Figure 5. SEM profile obtained after 60 s of etching using T2 recipe : (a) with nickel mask (b) with the chromium mask with the defect of mask transfer, and (c) the optimized lift-off providing the perfectly transferred nanopillar with chromium mask.

Among all possible materials, this study focuses on thin-metallic masks. As presented in Fig.4, these masks have interesting features, such as thermal conductivity, density, resistivity, Young modulus and integration with electronics. Moving from the micro- to the nanoscales requires a review of the selected materials. Gold (Au) because of its high electrical and thermal properties, is used as an electrical contact,but cannot be suited as a hard mask because this metal is a bad mask for plasma etching processes. We have selected chromium (Cr) and nickel (Ni) with high Young modulus(>200 GPa), as a hard-mask because of their high resistance to plasma etching and their low redeposition on the sample during the etching (low mass density (<10 g/cm^3), as seen in Fig.4).

In this technology process, the deposited thickness of each hard mask was 150 nm of Cr, or 100 nm of Ni and validated with a profilometer. The Cr masks presented straighter and smoother sidewalls and seem the most suited for chlorinated chemistry plasma etching. As expected, we have observed an increase in selectivity of Cr-masks compared to the photoresist mask. The Cr-mask has a lower etching rate (0.025 μm/min) compared to the AZ9260 photoresist mask in the same $BCl_3/Cl_2/Ar/N_2$ plasma chemistry. A selectivity > 60:1 is measured on the Cr mask for an 28 μm etching depth of and a pressure of 30 mTorr, compared to a selectivity of 16:1 on the photoresist mask in the same etching condition. The addition of the N_2 improves the sidewalls quality for the whole pressure range (10 mTorr - 30 mTorr). In Fig.3e, an under-etching is observable on top of the disk (dark layer). This defect is the recessing effect due to the use of a thin metallic mask for deeper etching. Concerning the surface morphology, we observed that GaAs etched using the photoresist mask and the Cr-mask was better in microscale using the T2-recipe.

However, at the nanoscale, the catalysis of the Ni mask occured at the top of each GaAs nanopillars as shown in Fig.5a. This catalysis of Ni has precedently been observed with other chemistries (Cl_2/N_2) by Jalabert *et al.* [20]. The use of Ni mask results in domed round head GaAs nano-pillars. For this reason, we have preferred the use of the Cr mask. However, Cr mask leads to residues on the sides of the mask which remain on the pattern after lift-off as it does not tear off well from the sidewalls of the pattern as shown in Fig.5b. This is a common problem with Cr which is exacerbated as the thickness of the mask is increased, especially at the nanoscale. The optimized lift-off presented in Fig.5c shows that we can provide a perfect transferred nanopillar with chromium mask.

4. Discussion

In this ICP- DRIE study, we have investigated both photoresist masks and metal masks during the etching processes: microfabrication was optimized to achieve straight, smooth sidewalls and a deeper depth, while the nanofabrication etching was improved to obtain the desired nanopillar shape. There are many parameters in the processing such as pressure, coil power/platen power and gas mixture, and we find that :

- Various demands on mask selectivity, etching rate and profile can be met in the fabrication of the III-V compounds based on this starting point recipes.
- Deep etching achieved at reasonably high etch rates using a thick photoresist mask provides better flexibility.
- A baseline on controlling the profile of microdevices and/or nanodevices opens a wide area of applications in one tool.

With these optimized processes we have successfully etched trenches ranging from 10 μm of width and 30 μm depth to 50 μm wide trenches with 117 μm depth. The results give an indication of the etching selectivities, with recommendations for the optimal choice of pattern transfer processes for each type of etch plasma chemistry during the manufacture of III-V devices. The micromachined micro-disks fabricated in this work have applications for terahertz microcavity lasers [6], as seen in Fig.6.

We highlight the effects of chlorine-based GaAs etch plasma chemistries on profile evolution and hence etch fidelity. Table I and Fig.1b present results of these trenches, which have been etched during 5 min. Low process pressure recipes (T1 and T2) are beneficial for high-aspect ratio etching, as exchange of

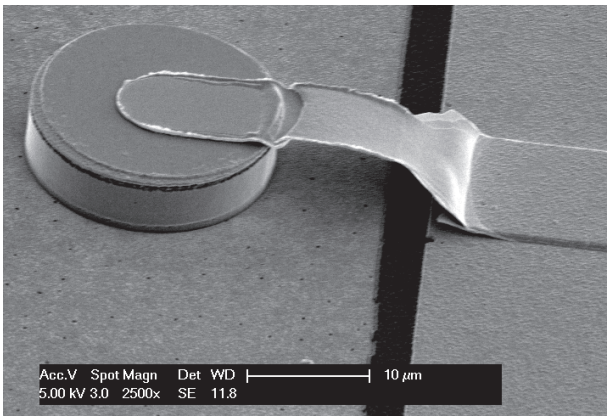

Figure 6. SEM image of the fabricated micro-disks using for terahertz micro-cavity lasers.

species in narrow deep trenches is accelerated by higher mean-free path of the gas molecules and radicals. However, at low pressure of 10 mTorr, mask selectivity gets degraded to 4:1 due to physical plasma etching with a lower etch rate as presented in Fig.1b, thus limiting the etch depths. Moreover, for the nanofabrication, processes at low pressure, for instance T1, causes a necking profile, while with an increasing BCl_3/Cl_2 ratio up to 20 :1 (T2), this necking effect was overcome.

For the photoresist and hard mask layers we compared the processing results of GaAs etching using the recipe T2. Table II summarizes the thickness, the etch rate and the selectivity of each targeted mask materials. When the selectivity is too low, a thicker mask is required to achieve the desired etching depths. For these reasons, deep GaAs etching requires higher selectivity masks. Ni shows a high selectivity for etching GaAs nanopillars but appears to be inadequate for some applications, for instance in the manufacturing of superconducting nanopillars [29]. However, the nanopillars with high aspect ratio often collapse due to over etching of the sidewalls at their base. Due to the better selectivity of Cr-mask, a thin mask layer was remaining after completed the GaAs etching at higher pressure. The profile was obtained with controlled under-etching as shown in Fig.7a which is shaped with a top diameter of 450±20 nm and a bottom diameter of 190±20 nm. Therefore, to protect sidewalls at higher pressures, it is required to increase N_2 flow rate to prevent lateral etching. A SEM image is presented in Fig.7b, using a Cr-mask, which shows a tall nanopillar obtained using the optimized etching process (T5). With a N_2 flow of 5 sccm, such a passivation layer prevents under-etching, leading to higher aspect ratios (e.g. 450 nm diameter and 5.6 μm tall GaAs nanopillar). Nevertheless, for N_2 flow rate >5 sccm at lower pressure (20 mTorr), the addition can cause micromasking (rough surface) due to the passivation effect. The verticality of the etching profile decreases with the increasing in etching time but the mechanical stability of the nanopillars is unaffected up to 100 seconds.

Table 2. Comparison of the different masks used in our work using an ICP-DRIE reactor with the T2 recipe.

Mask	AZ4562	Cr	Ni
Thickness (μm)	6	0.15	0.2
Mask etching rate (μm/min)	0.34-0.45	0.05	0.02
Selectivity	4-16	60	75

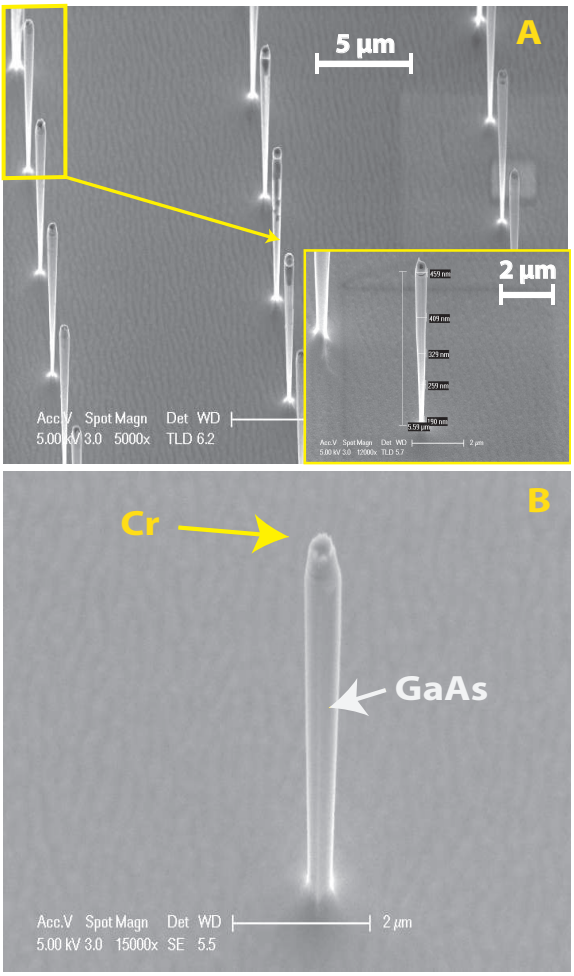

Figure 7. Cross-sectional SEMs, taken at 45° of high aspect ratio GaAs nanopillars at 30 mTorr of a) 4.14 μm tall GaAs nanopillar with the inset shows a closeup, and b) 450 nm diameter and 5.6 μm tall GaAs nanopillar.

In Table III, we have presented the manufacture of GaAs nanopillars into two approaches: dry etching and wet etching by using an ICP-RIE and MacEtch technology respectively. Unlike the ICP-RIE, the Mactech technology is essentially a wet etching based system with mechanisms involving a localized electrochemical process. The latter can achieve anisotropic high aspect ratio GaAs micro and nanostructures. However, the sidewall is rougher than ICP-DRIE technology using chlorinated chemistry [45].

In addition, the performances of III-V devices depend on the geometry of the cavity (coupling with the electromagnetic field) and the thickness of the active region (overlap with the electromagnetic fields). Thick heterostructures (>20 μm) are

Table 3. Comparison of different GaAs dry etching techniques.

Reference	Reference [29]	Reference[21]	Reference [20]	Reference[45]	Our work
Lithography	EBL	EBL	EBL	EBL	EBL
Dry technology	ICP-RIE	ICP-RIE	ICP-RIE	MacEtch	ICP-RIE
Combined with	——	——	——	wet etching	——
Mask	Al/Cr	Al	Ni	Au	Cr
Temperature	20 °C	20 °C	20-45 °C	40-45 °C	25°C
Chemistry	Cl_2/N_2	$BCl_3/Cl_2/Ar/N_2$	Cl_2/N_2	H_2SO_4 /$KMnO_4$	$BCl_3/Cl_2/Ar/N_2$
Diameter (nm)	50-400	520	30	500-1000	450-550
GaAs etching rate (μm/min)	0.1	1.5	> 5	1-2	> 5
Height (μm) of GaAs	2.2	2.85	1	< 3.5	> 5

achievable with long epitaxy time [46] or wafer-bonding of active regions [47]. However, the heterostructure thickness results generally in a cavity geometry with a high aspect ratio that is challenging to fabricate. The high aspect ratio is particularly critical for the etching of the active region, and a good combination mask/recipe is required to obtain a high quality etching with vertical and smooth sidewalls.

This engineering work delivers methodologies, processes, and tools to enable the efficient integration and exploitation of GaAs compound technologies. We provide the manufacturing and development of micro-and nano-technology-based devices and chlorinated plasma chemistry in order to increase devices reliability. These investigations also bring more attention in the selective etching processes for other III-V semiconductor compounds with potential applications in the manufacturing of the optoelectronic devices and microsystems MEMS and MOEMS. We believe that the present findings offer a new platform for novel approaches to achieve efficiency and reliable manufacturing.

5. Conclusion

This work reports on an optimized ICP etching process at the micrometer and nanometer scale of GaAs substrate through our optimized $BCl_3/Cl_2/Ar/N_2$ plasma chemistries conditions. For microdevices manufacturing where straight and smooth sidewalls are requested, the photoresist masks or Cr-masks have better results than Ni-mask. We highlighted the selection of the hard mask properties towards the nanoscale, and some interesting effects may arise. In particular, for the manufacturing of nano-scale devices, a Cr-mask is necessary to increase the selectivity as well as to reduce the surface roughness. The work done here paves the way towards achieving microdevices and nanodevices using III-V semiconductor compounds for various applications in microelectronics, microsystems and optoelectronics.

Acknowledgment

The authors acknowledge the clean room and characterization laboratory staff. This work was partly supported by the French RENATECH network with technological facilities. They also would like to thank David Bouville and Samson Edmond for fruitful discussions.

References

[1] Pires B, Silva A, Moskaltsova A, Deepak F, Brogueira P, Leitao D, et al. Multilevel process on large area wafers for nanoscale devices. Journal of Manufacturing Processes 2018;32:222 – 229. http://www.sciencedirect.com/science/article/pii/S1526612518300240.

[2] Elbaz A, Buca D, von den Driesch N, Pantzas K, Patriarche G, Zerounian N, et al. Ultra-low-threshold continuous-wave and pulsed lasing in tensile-strained GeSn alloys. Nature Photonics 2020;14:375–382. https://doi.org/10.1038/s41566-020-0601-5.

[3] Rainko D, Ikonic Z, Elbaz A, von den Driesch N, Stange D, Herth E, et al. Impact of tensile strain on low Sn content GeSn lasing. Scientific Reports 2019;9(1):259. https://doi.org/10.1038/s41598-018-36837-8.

[4] Herth E, Algré E, Rauch JY, Gerbedoen JC, Defrance N, Delobelle P. Modeling and characterization of piezoelectric beams based on an aluminum nitride thin-film layer. Physica Status Solidi A 2015;213(1):114–121. https://www.onlinelibrary.wiley.com/doi/abs/10.1002/pssa.201532302.

[5] Bajoni D, Senellart P, Wertz E, Sagnes I, Miard A, Lemaître A, et al. Polariton laser using single micropillar GaAs-GaAlAs semiconductor cavities. Physical Review Letters 2008;100(4):047401. https://link.aps.org/doi/10.1103/PhysRevLett.100.047401.

[6] Chassagneux Y, Palomo J, Colombelli R, Dhillon S, Sirtori C, Beere H, et al. Terahertz microcavity lasers with subwavelength mode volumes and thresholds in the milliampere range. Applied Physics Letters 2007;90(9):091113. https://aip.scitation.org/doi/full/10.1063/1.2710754.

[7] Tchernycheva M, Harmand JC, Patriarche G, Travers L, Cirlin GE. Temperature conditions for GaAs nanowire formation by Au-assisted molecular beam epitaxy. Nanotechnology 2006;17(16):4025–4030. https://doi.org/10.1088%2F0957-4484%2F17%2F16%2F005.

[8] Larrue A, Belharet D, Dubreuil P, Bonnefont S, Gauthier-Lafaye O, Monmayrant A, et al. Inductively coupled plasma etching of high aspect ratio two-dimensional photonic crystals in Al-rich AlGaAs and AlGaAsSb. Journal of Vacuum Science & Technology B 2011;29(2):021006. https://avs.scitation.org/doi/full/10.1116/1.3549125.

[9] Chiu HC, Chen CH, Kao HL, Chien FT, Weng PK, Gau YT, et al. Sidewall defects of AlGaN/GaN HEMTs evaluated by low frequency noise analysis. Microelectronics Reliability 2013;53(12):1897–1900. http://www.sciencedirect.com/science/article/pii/S0026271413001686.

[10] Kim JK, Lee JH, Joo YW, Park YH, Noh HS, Lee JW, et al. Nonselective vertical etching of GaAs and AlGaAs/GaAs in high pressure capacitively coupled BCl_3/N_2 plasmas. Current Applied Physics 2010;10(2):416–418. http://www.sciencedirect.com/science/article/pii/S1567173909003332.

[11] Landesman JP, Levallois C, Jiménez J, Pommereau F, Léger Y, Beck A, et al. Evidence of chlorine ion penetration in InP/InAsP quantum well structures during dry etching processes and effects of induced-defects on the electronic and structural behaviour. Microelectronics Reliability 2015;55(9):1750–1753. http://www.sciencedirect.com/science/article/pii/S0026271415301153.

[12] Herth E, Baranski M, Berlharet D, Edmond S, Bouville D, Calvet LE, et al. Fast ultra-deep silicon cavities: Toward isotropically etched spherical silicon molds using an ICP-DRIE. Journal of Vacuum Science & Technology B 2019;37(2):021206. https://doi.org/10.1116/1.5081503.

[13] Herth E, Valbin L, Lardet-Vieudrin F, Algré E. Modeling and detecting response of micromachining square and circular membranes transducers based on AlN thin film piezoelectric layer. Microsystem Technology 2015;23(9):3873–3880. https://doi.org/10.1007/s00542-015-2727-9.

[14] Herth E, Edmond S, Bouville D, Cercus JL, Bayle F, Cambril E. Micro-nanopillars for micro- and nanotechnologies using inductively coupled plasmas. Physica Status Solidi (a) 2019;216(23):1900324. https://onlinelibrary.wiley.com/doi/abs/10.1002/pssa.201900324. arXiv:https://onlinelibrary.wiley.com/doi/pdf/10.1002/pssa.201900324. http://www.sciencedirect.com/science/article/pii/S0167931709005322.

[15] Roland I, Masson S, Ducloux O, Traon OL, Bosseboeuf A. Gaas-based tuning fork microresonators: A first step towards a GaAs-based coriolis 3-axis micro-vibrating rate gyro (gaas 3-axis μcvg). Sensors and Actuators A: Physics 2011;172(1):204 – 211. http://www.sciencedirect.com/science/article/pii/S0924424711004213.

[16] Lacour V, Herth E, Lardet-Vieudrin F, Dubowski JJ, Leblois T. GaAs based on bulk acoustic wave sensor for biological molecules detection. Procedia Engineering 2015;120:721–726. http://www.sciencedirect.com/science/article/pii/S1877705815024352.

[17] Donnelly VM, Kornblit A. Plasma etching: Yesterday, today, and tomorrow. Journal of Vacuum Science & Technology A 2013;31(5):050825. https://avs.scitation.org/doi/full/10.1116/1.4819316.

[18] Xu G, Li L, Isac N, Halioua Y, Giles Davies A, Linfield EH, et al. Surface-emitting terahertz quantum cascade lasers with continuous-wave power in the tens of milliwatt range. Applied Physics Letters 2014;104(9):091112. https://aip.scitation.org/doi/abs/10.1063/1.4866661.

[19] Wang F, Nong H, Fobbe T, Pistore V, Houver S, Markmann S, et al. Short terahertz pulse generation from a dispersion compensated modelocked semiconductor laser. Laser Photonics Rev 2017;11(4). http://onlinelibrary.wiley.com/doi/10.1002/lpor.201700013/abstract.

[20] Jalabert L, Dubreuil P, Carcenac F, Pinaud S, Salvagnac L, Granier H, et al. High aspect ratio GaAs nanowires made by ICP-RIE etching using Cl_2/N_2 chemistry. Microelectronic Engineering 2008;85(5):1173–1178. http://www.sciencedirect.com/science/article/pii/S0167931708000646. doi:10.1016/j.mee.2008.01.063.

[21] Volatier M, Duchesne D, Morandotti R, Arès R, Aimez V. Extremely high aspect ratio GaAs and GaAs/AlGaAs nanowaveguides fabricated using chlorine ICP etching with N_2-promoted passivation. Nanotechnology 2010;21(13):134014. http://stacks.iop.org/0957-4484/21/i=13/a=134014. doi:10.1088/0957-4484/21/13/134014.

[22] Rawal SD, Kapoor A, Sharma SH, Sehgal KB, Malik KH. A highly selective low pressure inductively coupled plasma etching process for GaAs using photoresist mask. The Open Plasma Physics Journal 2011;4(1). https://benthamopen.com/ABSTRACT/TOPPJ-4-34.

[23] Liu K, Ren Xm, Huang Yq, Cai Sw, Duan Xf, Wang Q, et al. Inductively coupled plasma etching of GaAs in Cl_2/Ar, Cl_2/Ar/O_2 chemistries with photoresist mask. Applied Surface Science 2015;356:776–779. http://www.sciencedirect.com/science/article/pii/S016943321501819X.

[24] Shul RJ, McClellan GB, Briggs RD, Rieger DJ, Pearton SJ, Abernathy CR, et al. High-density plasma etching of compound semiconductors. Journal of Vacuum Science & Technology A 1997;15(3):633–637. https://avs.scitation.org/doi/10.1116/1.580696.

[25] Rawal DS, Malik HK, Sehgal BK, Muralidharan R. Study of Cl_2/BCl_3 inductively coupled plasma for selective etching of GaAs. In: 2009 IEEE International Conference on Plasma Science - Abstracts. 2009, p. 1–1.

[26] Edwards GT, Sobiesierski A, Westwood DI, Smowton PM. Fabrication of high-aspect-ratio, sub-micron gratings in AlGaInP/GaAs laser structures using a BCl_3/Cl_2/Ar inductively coupled plasma. Semiconductor Science Technology 2007;22(9):1010. http://stacks.iop.org/0268-1242/22/i=9/a=006.

[27] Constantine C, Shul RJ, Sullivan CT, Snipes MB, McClellan GB, Hafich M, et al. Etching of GaAs/AlGaAs rib waveguide structures using $BCl_3/Cl_2/N_2$/Ar electron cyclotron resonance. Journal of Vacuum Science & Technology B 1995;13(5):2025–2030. https://avs.scitation.org/doi/10.1116/1.588128.

[28] Lee JW, Devre MW, Reelfs BH, Johnson D, Sasserath JN, Clayton F, et al. Advanced selective dry etching of GaAs/AlGaAs in high density inductively coupled plasmas. Journal of Vacuum Science & Technology A 2000;18(4):1220–1224. https://avs.scitation.org/doi/abs/10.1116/1.582329.

[29] Dhindsa N, Chia A, Boulanger J, Khodadad I, LaPierre R, Saini SS. Highly ordered vertical GaAs nanowire arrays with dry etching and their optical properties. Nanotechnology 2014;25(30):305303. http://stacks.iop.org/0957-4484/25/i=30/a=305303.

[30] Park YH, Kim JK, Lee JH, Joo YW, Noh HS, Lee JW, et al. N_2 effect on GaAs etching at 150 mtorr capacitively-coupled Cl_2/N_2 plasma. Microelectronics Engineering 2010;87(4):548–552. http://www.sciencedirect.com/science/article/pii/S0167931709005322.

[31] Heo W, Lee NE. Effect of additive N_2 and ar gases on surface smoothening and fracture strength of si wafers during high-speed chemical dry thinning. Microelectronics Reliability 2012;52(2):412–417. http://www.sciencedirect.com/science/article/pii/S0026271411004355.

[32] Vigneron PB, Joint F, Isac N, Colombelli R, Herth E. Advanced and reliable GaAs/AlGaAs ICP-DRIE etching for optoelectronic, microelectronic and microsystem applications. Microelectronics Engineering 2018;202:42–50. http://www.sciencedirect.com/science/article/pii/S0167931718303848.

[33] Kovacs GTA, Maluf NI, Petersen KE. Bulk micromachining of silicon. Proc IEEE 1998;86(8):1536–1551.

[34] Franz G, Hösler W, Treichler R. Sidewall passivation of GaAs in BCl_3-containing atmospheres. Journal of Vacuum Science & Technology B 2001;19(2):415–419. https://avs.scitation.org/doi/abs/10.1116/1.1347045.

[35] Lee KH, Guilet S, Patriarche G, Sagnes I, Talneau A. Smooth sidewall in InP-based photonic crystal membrane etched by N_2-based inductively coupled plasma. Journal of Vacuum Science & Technology B 2008;26(4):1326–1333. https://avs.scitation.org/doi/abs/10.1116/1.2945299.

[36] Mouffak Z, Bensaoula A, Trombetta L. The effects of nitrogen plasma on reactive-ion etching induced damage in GaN. Journal of Applied Physics 2004;95(2):727–730. https://doi.org/10.1063/1.1632552.

[37] Signorello G, Karg S, Björk MT, Gotsmann B, Riel H. Tuning the light emission from GaAs nanowires over 290 meV with uniaxial strain. Nano Letters 2013;13(3):917–924. https://doi.org/10.1021/nl303694c.

[38] Chao JJ, Wang DS, Shiu SC, Hung SC, Lin CF. Controlled formation of well-aligned GaAs nanowires with a high aspect ratio on transparent substrates. Semiconductor Science and Technology 2010;25(6):065014. http://stacks.iop.org/0268-1242/25/i=6/a=065014.

[39] Kapadia R, Fan Z, Takei K, Javey A. Nanopillar photovoltaics: Materials, processes, and devices. Nano Energy 2012;1(1):132–144. http://www.sciencedirect.com/science/article/pii/S2211285511000188.

[40] Guisbiers G, Herth E, Legrand B, Rolland N, Lasri T, Buchaillot L. Materials selection procedure for RF-MEMS. Microelectronics Engineering 2010;87(9):1792–1795. http://www.sciencedirect.com/science/article/pii/S016793170900608X.

[41] Gorelick S, Guzenko VA, Vila-Comamala J, David C. Direct e-beam writing of dense and high aspect ratio nanostructures in thick layers of pmma for electroplating 2010;21:295303. doi:10.1088/0957-4484/21/29/295303.

[42] Yasin S, Hasko D, Ahmed H. Comparison of mibk/ipa and water/ipa as pmma developers for electron beam nanolithography. Microelectronic engineering 2002;61:745–753.

[43] Herth E, Algre E, Tilmant P, Francois M, Boyaval C, Legrand B. Performances of the negative tone resist aznlof 2020 for nanotechnology appli-

cations 2012;11:854–859. doi:10.1109/tnano.2012.2196802.

[44] Yang H, Jin A, Luo Q, Li J, Gu C, Cui Z. Electron beam lithography of hsq/pmma bilayer resists for negative tone lift-off process. Microelectronic Engineering 2008;85(5-6):814–817.

[45] DeJarld M, Shin JC, Chern W, Chanda D, Balasundaram K, Rogers JA, et al. Formation of high aspect ratio GaAs nanostructures with metal-assisted chemical etching. Nano Letters 2011;11(12):5259–5263. https://doi.org/10.1021/nl202708d.

[46] Li L, Chen L, Zhu J, Freeman J, Dean P, Valavanis A, et al. Terahertz quantum cascade lasers with¿ 1 w output powers. Electronics letters 2014;50(4):309–311.

[47] Brandstetter M, Deutsch C, Krall M, Detz H, MacFarland DC, Zederbauer T, et al. High power terahertz quantum cascade lasers with symmetric wafer bonded active regions. Applied Physics Letters 2013;103(17):171113. https://doi.org/10.1063/1.4826943. doi:10.1063/1.4826943. arXiv:https://doi.org/10.1063/1.4826943.